JOURNAL OF GEOPHYSICAL RESEARCH, VOL. 96, NO. B5, PAGES 8045–8055, MAY 10, 1991

Analysis of Geoid Height Versus Topography for Oceanic Plateaus and Swells Using Nonbiased Linear Regression

KAREN M. MARKS[1]
Department of Geosciences, University of Houston, Houston, Texas

DAVID T. SANDWELL
Scripps Institution of Oceanography, La Jolla, California

We have investigated the relationship between geoid height and topography for 53 oceanic plateaus and swells to determine the mode of compensation. The ratio of geoid height to topography was obtained from the slope of a best line fit by functional analysis (i.e. nonbiased linear regression), a method that minimizes both geoid height and topography residuals. This method is more appropriate than traditional least squares analysis that minimizes only geoid height residuals, because uncertainties are present in both data types. We find that approximately half of the oceanic and continental plateaus analyzed have low ratios that are consistent with Airy-compensated crustal thickening. The remaining plateaus, however, have higher geoid/topography ratios than predicted by the simple Airy model, and the seismically determined Moho depths beneath some of these features are too shallow for crustal thickening alone. A two-layer Airy compensation model, composed of thickened crust underlain by an anomalously low density "mantle root," is used to explain these observations. The Walvis Ridge, and the Agulhas, Crozet, and north Kerguelen plateaus have geoid/topography ratios and Moho depths that are consistent with the two-layer Airy model. The proximity of the Agulhas Plateau to a RRR triple junction during its early development, and the excessive volcanism at active spreading ridges that created the Crozet and north Kerguelen plateaus and the Walvis Ridge, may have produced regions of enhanced depletion and hence the low-density mantle anomalies. If this explanation is correct, then the low-density mantle anomaly persists over time and remains embedded in the lithosphere beneath the oceanic feature.

INTRODUCTION

Sandwell and MacKenzie [1989] investigated the relationship between geoid height and topography to determine the mode of compensation for 53 oceanic plateaus and swells (Figure 1). Two local isostatic compensation models were considered in their analysis, that of crustal thickening (Airy compensation) and that of lithospheric thinning (thermal compensation). They found that most of the oceanic and continental plateaus have low geoid/topography ratios (0-2 m/km) that are roughly compatible with Airy-compensated crustal thickening. The thermal swells were found to have intermediate geoid/topography ratios (2-6 m/km), which they attributed to a combination of decaying thermal compensation in the lower lithosphere and shallow Airy compensation of the volcanic edifice.

The geoid/topography ratios were obtained by plotting geoid height against topography and calculating the slope of the best fit line using a traditional least squares method. In this method, all uncertainties are assumed to reside in the geoid height data, and the line therefore minimizes the sum of the squares of the geoid height residuals. In the research presented here, we propose that it is more appropriate to assume that uncertainties are contained in both the geoid height and topography data. The best fit line therefore minimizes both geoid height and topography residuals, and is obtained from functional analysis (i.e., nonbiased linear regression) [*Mark and Church*, 1977].

Using this nonbiased linear regression method, we have calculated the geoid/topography ratios for the 53 plateaus and swells previously analyzed by *Sandwell and MacKenzie* [1989]. Unlike their study, which suggested that most oceanic plateaus were in accordance with the simple Airy compensation model, our results show that only approximately half of the oceanic and continental plateaus have low geoid/topography slopes that are consistent with Airy-compensated crustal thickening. We find that the remaining plateaus have higher geoid/topography slopes than predicted by the simple Airy model, and the seismically determined Moho depths beneath some of these features (the aseismic ridges) are too shallow for thickened crust alone. The excessive volcanism at active spreading ridges that creates aseismic ridges [*Goslin and Patriat*, 1984] may produce regions of enhanced depletion and hence low-density mantle anomalies beneath these features. We therefore investigate a two-layer Airy compensation model, composed of thickened crust underlain by an anomalously low density "mantle root" [*Angevine and Turcotte*, 1983], to explain these observations. We find that the geoid/topography ratios associated with aseismic ridges match those predicted by the two-layer Airy model. The geoid/topography ratios we obtain for the thermal swells are significantly higher than those computed by *Sandwell and MacKenzie* [1989], and for the Hawaiian and Cape Verde swells in particular, these ratios are more consistent with those obtained using full spectral methods [e.g., *Courtney and White*, 1986; *McNutt and Shure*, 1986]. The nonbiased linear regression method therefore provides more accurate estimates of the geoid/topography ratios associated with oceanic plateaus and swells, and hence a better understanding of their origin and mechanism of compensation.

[1]Now at NOAA, National Geodetic Survey, Rockville, Maryland

Paper number 91JB00240.
0148-0227/91/91JB-00240$05.00

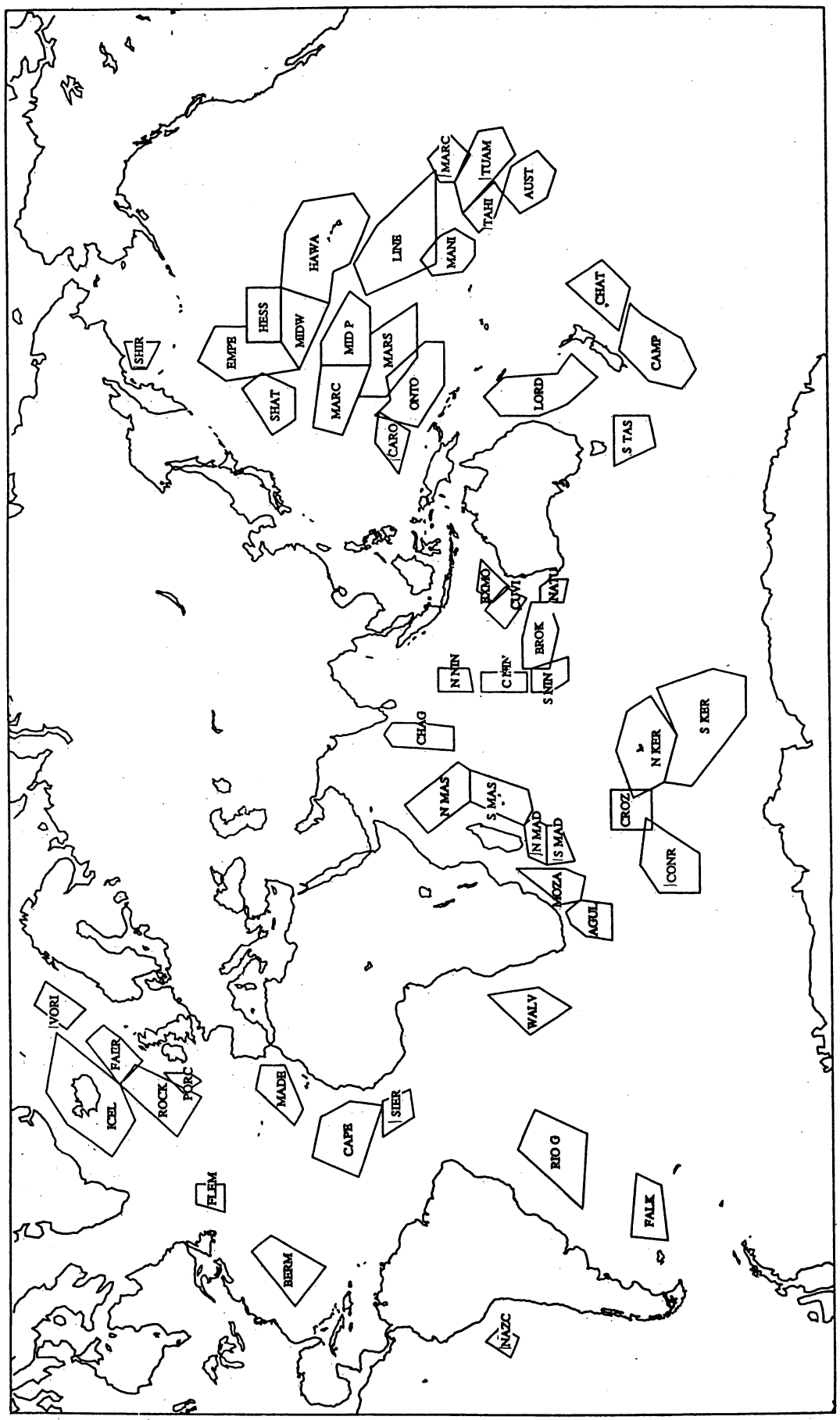

Fig. 1. Locations of oceanic features for geoid height versus topography analysis.

MODELS

We consider the two-layer Airy model first proposed by *Angevine and Turcotte* [1983] to explain the higher geoid/topography ratios. The two-layer Airy model is similar to the usual Airy model in that a water layer (ρ_w = 1025 kg m^{-3}) overlies a crustal layer (ρ_c = 2800 kg m^{-3}) and a half-space of undepleted mantle (ρ_m = 3300 kg m^{-3}). The additional feature is a layer of depleted mantle (ρ_l = 3240 kg m^{-3}) that forms when basaltic crustal material is extracted from the undepleted mantle [*Oxburgh and Parmentier*, 1977].

Figure 2 shows an oceanic plateau that is elevated a distance h above the surrounding seafloor and is isostatically compensated by both the thickened crustal layer (r) and the thickened depleted mantle layer (t). The mass balance is

$$(\rho_c - \rho_w)h = (\rho_m - \rho_c)r + (\rho_m - \rho_l)t$$

For the simple Airy model, the thickness of the depleted layer is zero (i.e., t=0), and the thickness of the Airy root is

$$r = \frac{(\rho_c - \rho_w)}{(\rho_m - \rho_c)}h$$

For the two-layer model, we let λ be the fraction of compensation associated with the Airy root, so that its thickness is λr, where λ ranges from 0 to 1. The remainder of the compensation is placed in the depleted layer, which has a thickness given by

$$t = \frac{(\rho_c - \rho_w)}{(\rho_m - \rho_l)}(1 - \lambda)h$$

Thus, given the elevation of the plateau, the fraction of Airy compensation (λ), and the assumed densities, the thickness of the crustal root and the thickness of the depleted mantle layer are uniquely determined.

The geoid height N is obtained from the long-wavelength approximation of isostatically compensated topography

$$N = -\frac{2\pi G}{g}\int_0^h z\,\Delta\rho(z)\,dz$$

[*Ockendon and Turcotte*, 1977]. We integrate the density configuration of the two-layer model over depth to obtain the following formula, which is functionally equivalent to the formula given by *Angevine and Turcotte* [1983]:

$$N = \frac{2\pi G}{g}(\rho_c - \rho_w)h \cdot \left\{z_c - z_w + \frac{h}{2}\left[1 + (2\lambda - \lambda^2)\frac{(\rho_c - \rho_w)}{(\rho_m - \rho_c)} + (1-\lambda)^2\frac{(\rho_c - \rho_w)}{(\rho_m - \rho_l)}\right]\right\}$$

where G is the gravitational constant, g is the acceleration of gravity, z_w (5 km) is the normal seafloor depth away from the plateau, and z_c (12 km) is the normal depth to the Moho. Note that when λ = 1, this geoid height model reduces to the simple Airy compensation model given by *Haxby and Turcotte* [1978]. The above equation shows that the square of the topography contributes to the predicted geoid signal. This contribution is small, however, and is not evident in the observed geoid/topography ratios (see next section). We therefore linearize the above equation by taking the average ratio over the topographic range (0 to h_{max}):

$$\frac{\Delta N}{\Delta h} = \frac{2\pi G}{g}(\rho_c - \rho_w) \cdot \left\{z_c - z_w + \frac{h_{max}}{2}\left[1 + (2\lambda - \lambda^2)\frac{(\rho_c - \rho_w)}{(\rho_m - \rho_c)} + (1-\lambda)^2\frac{(\rho_c - \rho_w)}{(\rho_m - \rho_l)}\right]\right\} \quad (1)$$

where h_{max} is the height of the plateau above the seafloor. Plots of geoid height versus topography for the simple Airy model and the two-layer Airy model (λ = 0.5) are shown in Figure 3. The two-layer Airy model predicts ratios that are systematically higher than those for simple Airy compensation.

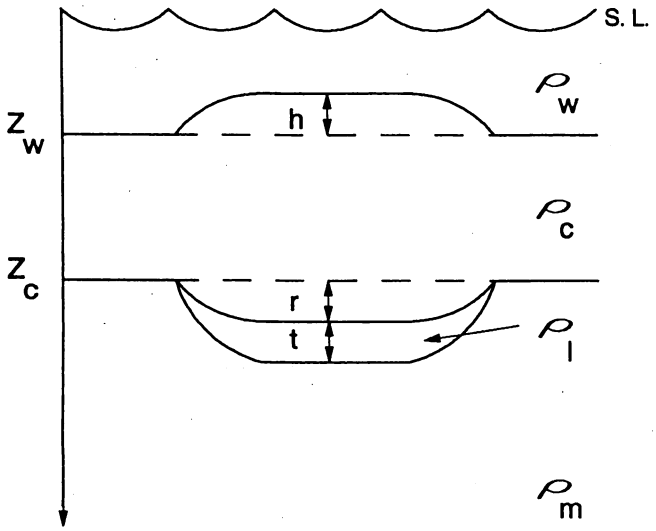

Fig. 2. Airy compensation model. The height of the plateau above the seafloor is h, the crustal root is r, and the mantle root is t. z_w is the water depth, and z_c the crustal depth, measured from sea level.

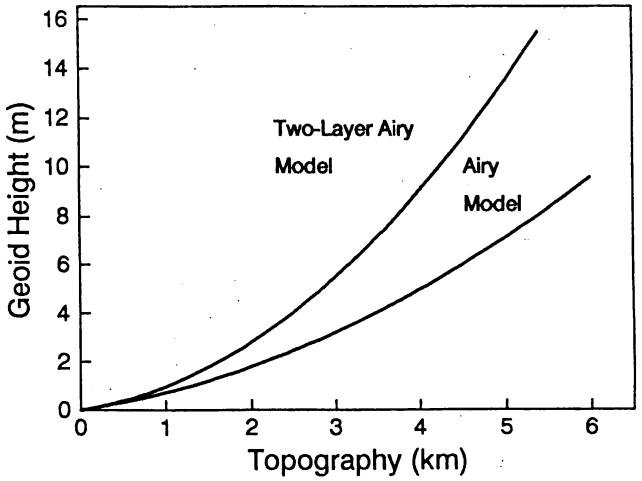

Fig. 3. Geoid height versus topography predicted from the Airy model (compensation entirely by a crustal root) and the two-layer Airy model (compensation half by crustal root and half by mantle root.).

For the present global analysis, we do not vary the densities (ρ_w, ρ_c, ρ_l, and ρ_m) for the different areas and, furthermore, make the assumption that the oceanic features are perfectly compensated. We thus interpret the variations in the observed geoid/topography ratios as reflecting the different modes of compensation.

METHOD

Gridded geoid height [*Marsh et al.*, 1986] and bathymetry data [*Van Wykhouse*, 1973] were used in this analysis. Both data sets were filtered to pass 400-4000 km wavelength anomalies [*Sandwell and MacKenzie*, 1989] because geoid height is nearly linearly related to topography in this wavelength band. Longer-wavelength (>4000 km) geoid and topography anomalies arise from density anomalies in the lower mantle [*Bowin*, 1983] and cooling of the lithosphere [*Haxby and Turcotte*, 1978], while shorter-wavelength (<400 km) anomalies contain signal from lithospheric flexure and variations in crustal thickness. These data are band-pass filtered to remove contamination from these unwanted signals and therefore reflect the local compensation mechanism.

The ratio of geoid height to topography is obtained by plotting the filtered geoid heights against filtered topography and calculating the slope of the best fit line. Traditionally, this is accomplished using linear regression, where geoid height is regressed on topography. The assumption is made that the topography data are uncertainty-free and the geoid height data are not, i.e., the x axis (topography) is independent and the y axis (geoid height) is dependent. Thus the line minimizes the sum of the squares of the geoid height residuals.

Considering that the databases have been gridded from irregular and widely spaced ship tracks, in the case of topography, and from satellite passes that are very dense along-track yet widely spaced between passes, in the case of geoid height, it is not correct to assume that all uncertainties are contained in the geoid height data. It is more appropriate to assume that uncertainties are present in both data sets. However, the misfits between the straight line and the data points are much greater than the errors in either the geoid or the topography measurements. Thus, we believe that the misfits represent random departures from the model, or even inadequacies in the model, and to a smaller extent, the measurement errors. Under these conditions, the best fit line is obtained from functional analysis (i.e., nonbiased linear regression), where the straight line minimizes both geoid height and topography residuals [*Mark and Church*, 1977]. The best line thus minimizes the sum:

$$\sum_i [w(X_i)(x_i - X_i)^2 + w(Y_i)(y_i - Y_i)^2] \qquad (2)$$

where X_i, Y_i are the topography and geoid height observations, x_i, y_i are points on the best line $y_i = a + bx_i$, and $w(X_i)$, $w(Y_i)$ are the weights assigned to the observations [*Deming*, 1943].

Although it is clear that uncertainties are present in both data sets, the amount of uncertainty is not known, because it largely reflects random variations or even inadequacies in the model. We cannot therefore determine weights for $w(X_i)$ and $w(Y_i)$. However, we can consider the ratio $w(X_i)/w(Y_i)$ and make the reasonable assumption that the ratio equals a constant, c. The slope (b) of the best line is then

$$b = \{S_{yy} - cS_{xx} + [(S_{yy} - cS_{xx})^2 + 4cS_{xy}^2]^{1/2}\}/2S_{xy} \qquad (3)$$

where $S_{xx} = \sum_i (X_i - \langle X \rangle)^2$, $S_{yy} = \sum_i (Y_i - \langle Y \rangle)^2$, $S_{xy} = \sum_i (X_i - \langle X \rangle)(Y_i - \langle Y \rangle)$, and the terms in brackets are the mean values [*York*, 1966]. The difficulty arises in the estimation of c. Much has been written on the subject of estimating c [e.g., *York*, 1966; *Mark and Church*, 1977; *Jones*, 1979]; however, for our problem, where the uncertainties are unknown, the best estimate is obtained when $w(Y_i) = 1/S_{yy}$ and $w(X_i) = 1/S_{xx}$ [*Jones*, 1979]. Inserting this ratio into (3), the slope (b) reduces to a simple form:

$$b = \pm(S_{yy}/S_{xx})^{1/2}$$

where the correct sign is obtained from S_{xy}. This best line is called the "reduced major axis" [*Kermack and Haldane*, 1950].

If there are no uncertainties in X_i, then $(x_i - X_i)$ goes to zero in (2), and the best line minimizes the sum of the squares of the geoid height residuals. Similarly, if there are no uncertainties in Y_i, then the second term in (2) goes to zero, and the best line minimizes the sum of the squares of the topography residuals. The first case yields the lowest possible slope, and the latter the highest possible slope. The reduced major axis always lies between the lines having the highest and lowest slopes. Yet the lowest slope is that traditionally used to obtain the ratios of geoid height to topography! We propose that the slope obtained from the least squares method that assumes uncertainties are present in both data sets provides the best estimate of the geoid height/topography ratio. We define the error in the slope of the reduced major axis as the difference between the highest and lowest slopes divided by the slope of the reduced major axis. The slopes of the three best lines (the geoid/topography ratios), the errors, and the maximum plateau heights for each of the 53 regions analyzed are listed in Table 1.

DISCUSSION

Plots of geoid height versus topography for the 53 regions, and the best lines computed from the three least square methods, are shown in Figure 4. Each plot shows the reduced major axis lying between the best lines having the lowest (shallowest) and highest (steepest) possible slopes. In some areas (for example, the Emperor and Marcus-Wake Seamounts), there are large differences between the highest and lowest slopes. These large discrepancies may be due to poor data quality, failure to obtain samples from a wide enough range of topographic depths (or geoid heights), or scatter that masks the linear correlation between geoid height and topography. Accordingly, we chose errors of $\geq$1.5 m/km as probably reflecting these effects. The following oceanic features were therefore excluded from further analysis because their errors exceeded the cutoff: the Chagos-Laccadive Ridge, Emperor Seamounts, Exmouth Plateau, Faeroe Block, Madeira Rise, Manihiki Plateau, Marcus-Wake Seamounts, Marshall-Gilbert Seamounts, Mid Pacific Mountains, North and Central Ninetyeast Ridge, and the Rockall and Shirshov plateaus.

Geoid/topography ratios for the remaining features are plotted against plateau height in Figure 5. Thermal swells of known or suspected hotspot origin are marked with triangles, and oceanic and continental plateaus with circles. As may be expected, the thermal swells and plateaus form two relatively distinct groups. With few exceptions, the thermal swells are associated with intermediate to high geoid/topography ratios (~2-6 m/km) and low plateau heights (<3 km). Oceanic and continental plateaus, on the other hand, display lower geoid/topography ratios (0-2 m/km) for a wide range of plateau heights (1-5.5 km). The lower solid line in Figure 5 depicts the geoid/topography ratio

TABLE 1. Geoid Height Versus Topography Results

Plateau or Swell	Abbrev.	h_{max}	N/h_y	N/h_x	N/h_p	Error
Agulhas Plateau	AGUL	2.771	1.404	1.726	1.557	0.207
Austral Swell	AUST	1.736	2.056	4.974	3.198	0.912
Bermuda Swell	BERM	2.265	3.194	4.619	3.841	0.371
Broken Ridge	BROK	3.168	0.782	2.246	1.326	1.104
Campbell Plateau	CAMP	4.241	1.427	2.103	1.732	0.390
Cape Verde Rise	CAPE	2.818	4.315	5.264	4.765	0.199
Caroline Seamounts	CARO	3.440	1.145	2.929	1.831	0.974
Chagos-Laccadive Ridge	CHAG	3.669	0.896	4.095	1.916	1.670
Chatham Rise	CHAT	4.200	1.718	2.899	2.232	0.529
Conrad Rise	CONR	2.638	2.633	2.786	2.709	0.056
Crozet Plateau	CROZ	3.055	1.409	1.704	1.550	0.190
Cuvier and Wallaby Plateaus	CUVI	2.203	1.939	3.859	2.736	0.702
Emperor Seamounts	EMPE	3.012	0.351	16.304	2.391	6.672
Exmouth Plateau	EXMO	4.531	0.263	1.256	0.575	1.727
Faeroe Block	FAER	2.010	1.185	4.764	2.376	1.506
Falkland Plateau	FALK	4.294	1.285	1.584	1.427	0.210
Flemish Cap	FLEM	2.894	0.992	1.649	1.279	0.514
Hawaiian Swell	HAWA	2.674	3.759	5.542	4.564	0.391
Hess Rise	HESS	2.446	1.694	2.003	1.842	0.168
Iceland	ICEL	2.828	1.532	3.140	2.193	0.733
North Kerguelen Plateau	N KER	4.115	1.409	3.146	2.105	0.825
South Kerguelen Plateau	S KER	3.224	1.800	2.471	2.109	0.318
Line Swell	LINE	2.688	1.941	6.807	3.634	1.339
Lord Howe Rise	LORD	4.258	0.813	1.441	1.082	0.580
North Madagascar Ridge	N MAD	3.664	1.519	1.727	1.620	0.128
South Madagascar Ridge	S MAD	4.147	2.196	2.309	2.252	0.050
Madeira Rise	MADE	2.064	1.887	9.361	4.203	1.778
Manihiki Plateau	MANI	2.519	0.524	4.094	1.465	2.437
Marcus-Wake Seamounts	MARC	1.511	0.927	9.988	3.042	2.979
Marquesas Swell	MARQ	1.875	1.637	6.525	3.269	1.495
Marshall-Gilbert Seamounts	MARS	2.221	1.008	5.091	2.266	1.802
North Mascarene Plateau	N MAS	5.064	1.687	2.328	1.982	0.323
South Mascarene Plateau	S MAS	4.121	1.729	2.863	2.225	0.510
Mid Pacific Mountains	MID P	2.714	0.342	4.262	1.208	3.245
Midway Swell	MIDW	1.811	2.070	4.437	3.031	0.781
Mozambique Plateau	MOZA	2.550	1.814	2.173	1.986	0.181
Naturaliste Plateau	NATU	2.526	0.772	1.095	0.919	0.351
Nazca Ridge	NAZC	1.980	1.390	1.959	1.650	0.345
North Ninetyeast Ridge	N NIN	1.888	1.098	5.032	2.351	1.673
Central Ninetyeast Ridge	C NIN	2.509	0.990	3.830	1.947	1.459
South Ninetyeast Ridge	S NIN	2.037	0.711	1.172	0.913	0.505
Ontong-Java Plateau	ONTO	2.513	1.653	5.616	3.047	1.301
Porcupine Bank	PORC	3.197	0.799	0.923	0.859	0.144
Rio Grande Rise	RIO G	3.823	2.277	3.849	2.961	0.531
Rockall Plateau	ROCK	2.373	-0.173	-7.950	-1.172	6.636
Shatsky Rise	SHAT	3.041	0.758	2.104	1.263	1.066
Shirshov Plateau	SHIR	1.713	-1.008	-8.907	-2.996	2.637
Sierra Leone Rise	SIER	1.780	2.094	2.836	2.437	0.304
Tahiti Swell	TAHI	1.475	2.465	2.840	2.646	0.142
South Tasman Rise	S TAS	2.864	0.826	3.287	1.648	1.493
Tuamotu Archipelago	TUAM	3.187	0.690	1.233	0.922	0.589
Voring Plateau	VORI	1.295	0.577	0.947	0.740	0.500
Walvis Ridge	WALV	3.131	1.407	2.479	1.867	0.574

Parameters are the plateau height (h_{max}), ratio from least squares minimization of geoid height residuals (N/h_y), ratio from least squares minimization of topography residuals (N/h_x), ratio from nonbiased linear regression where both geoid height and topography residuals are minimized (N/h_p), and the error of the nonbiased ratio. The plateau heights are in kilometers, and the ratios and errors in meters per kilometer.

predicted by the simple Airy compensation model (equation (1), when $\lambda = 1$) for a crustal density of 2800 kg m^{-3}. About half of the observed low geoid/topography ratios are in accordance with this simple Airy isostasy model.

Sandwell and MacKenzie [1989] concluded in their analysis that most oceanic structures were reasonably well modeled by the simple Airy model. We cannot make the same conclusion, however. Our results show that approximately half of the oceanic

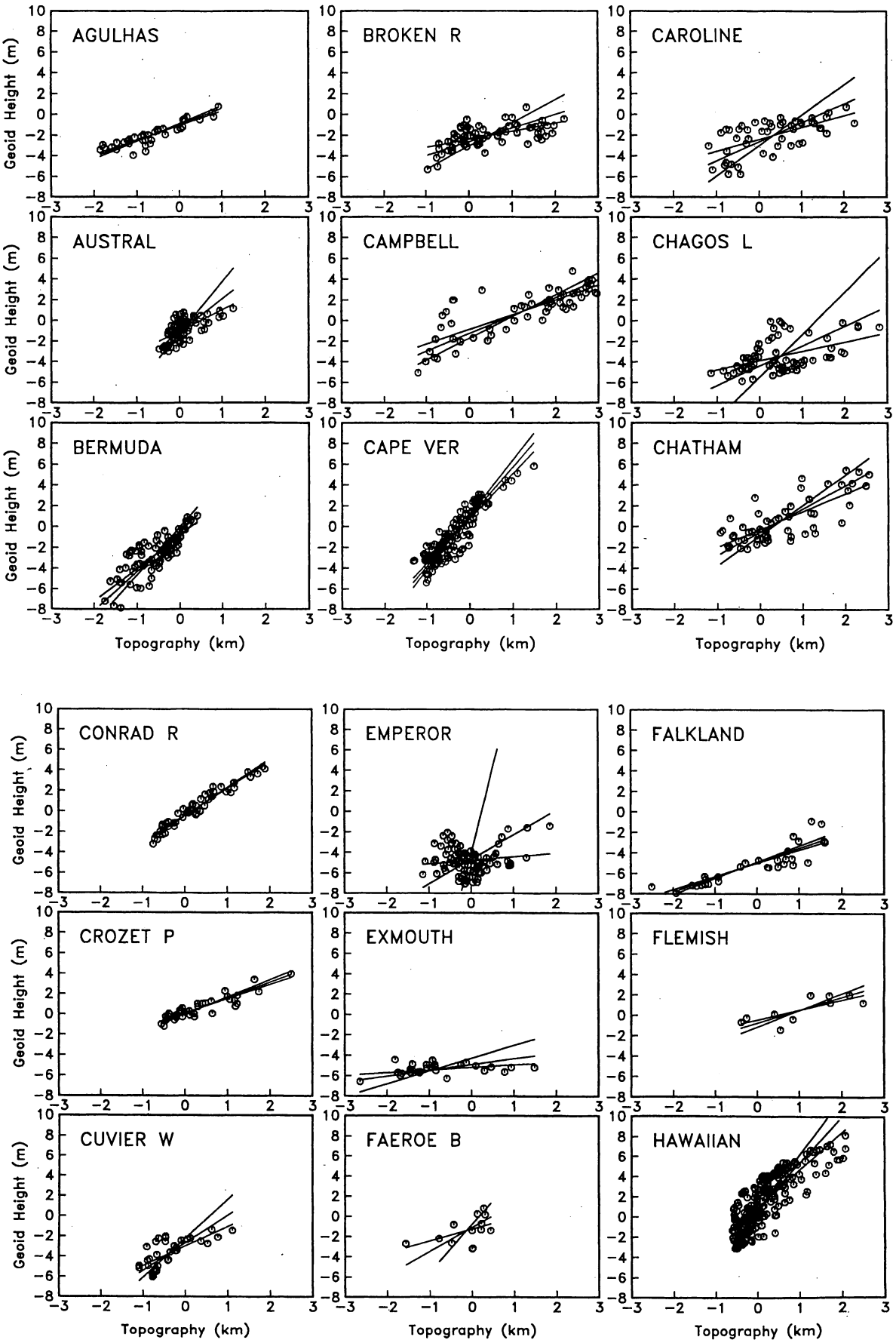

Fig. 4. Geoid height versus topography for the 53 oceanic features. Three best lines are plotted: all errors in geoid height data (shallowest slope), all errors in topography data (steepest slope), and errors in both data (intermediate slope).

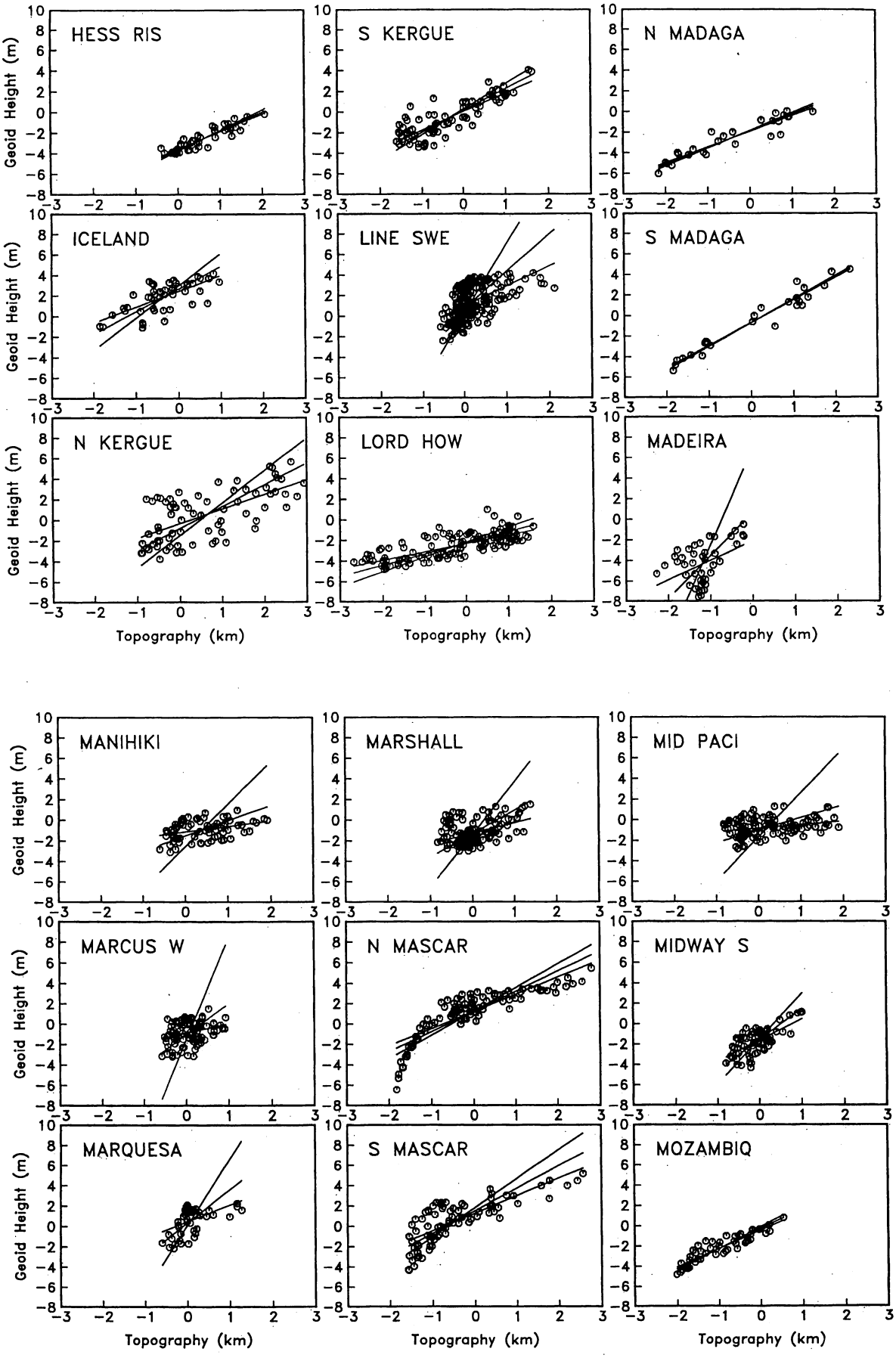

Fig. 4. (continued)

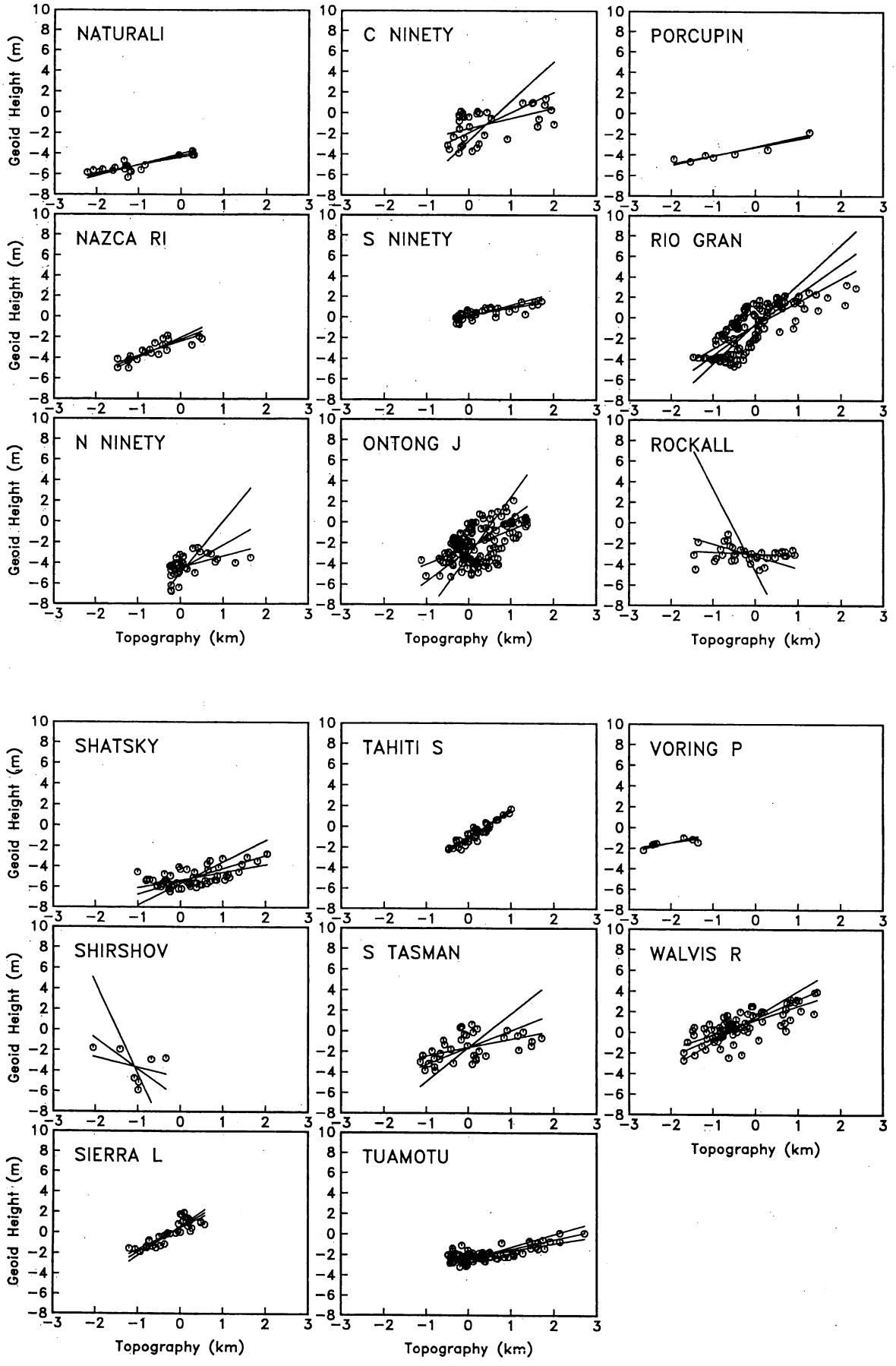

Fig. 4. (continued)

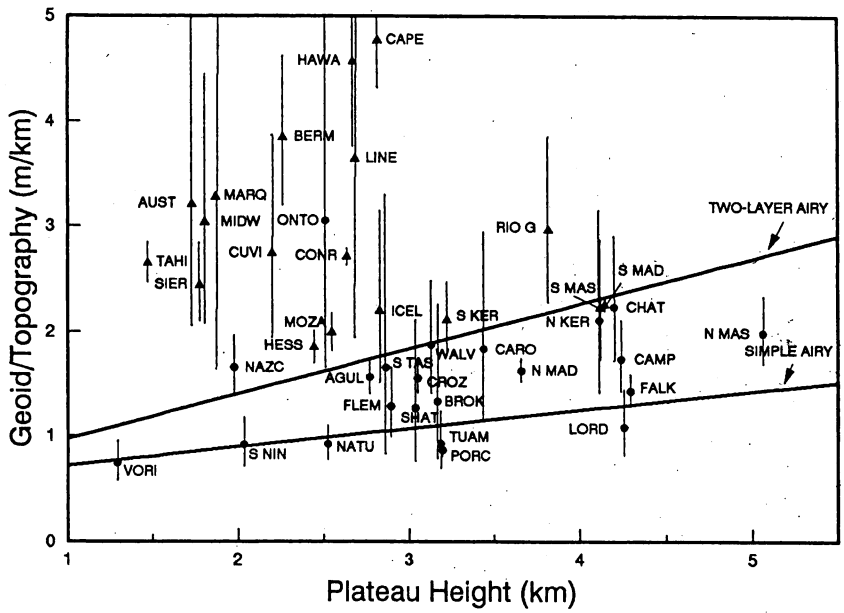

Fig. 5. The ratio of geoid height to topography plotted against plateau height. Triangles are thermal swells, and circles are oceanic and continental plateaus. Vertical lines bisecting the markers have the highest and lowest possible slopes as endpoints. The lower solid line is the ratio predicted from simple Airy compensation; the upper solid line is from the two-layer Airy model, where the compensation is half by crustal root and half by mantle root. Areas with errors of $\geq$1.5 m/km are omitted.

and continental plateaus analyzed have geoid/topography ratios that are significantly higher than predicted by the simple Airy model (Figure 5). For the simple Airy model to produce these higher ratios, unrealistically high crustal densities must be assumed.

We therefore investigate the more complex, two-layer Airy compensation model to explain the higher ratios (Figure 2). *Angevine and Turcotte* [1983] used this two-layer Airy model to describe the compensation of the Agulhas Plateau. Following *Oxburgh and Parmentier* [1977], they suggest excessive basalt generation beneath the plateau has produced depleted mantle that is anomalously light. This is consistent with the observations of *Dick et al.* [1984] that depleted mantle is associated with mantle thermal anomalies that cause excess basalt production. A two-layer model was able to simultaneously match the observed relationship between geoid height and topography and the shallow Moho depths (13-15 km) located by seismic refraction [*Tucholke et al.*, 1981]. *Angevine and Turcotte* did not compute the geoid/ topography ratio, but rather constrained the model parameters by plotting predicted curves against a simple plot of geoid height versus topography. Accordingly, their interpretation did not suffer from an improperly computed slope. Following their example, we used the two-layer Airy model (Figure 2) to interpret the 1.6 m/km geoid/topography ratio computed using the nonbiased linear regression method. Our results indicate the Agulhas Plateau is compensated by 18 km of thickened oceanic crust overlying a low-density mantle root that extends to a depth of 51 km. These results are in good agreement with those of *Angevine and Turcotte* [1983].

The crustal root ("r" in Figure 2) of the two-layer Airy model described above accounts for about 60% of the compensation (i.e., λ = 0.6 in equation (1)) of the Agulhas Plateau. We consider the possibility that other plateaus are likewise compensated by thickened crust and a mantle root, but that the portion of compensation due to the crustal (and mantle) root may vary. The upper solid line in Figure 5 shows the geoid/topography ratio predicted by the two-layer Airy compensation model, where half the compensation is due to the crustal root and half to the mantle root (λ = 0.5). With the exception of the Nazca Ridge and Ontong-Java Plateau, oceanic features having geoid/topography ratios higher than predicted by simple Airy compensation lie below this line. This suggests that the compensation of plateaus may range between entirely by crustal thickening (simple Airy model) to half crustal root and half mantle root (two-layer Airy model).

To test this idea, we interpret the high 1.9 m/km geoid/topography ratio computed for the Walvis Ridge in light of the two-layer Airy model. Our results indicate the Walvis Ridge may be compensated by oceanic crust 17.5 km thick overlying anomalously low density mantle to depths of 64 km. A Rayleigh wave inversion for the Walvis Ridge [*Chave*, 1979] suggests a crustal thickness of 12.5 $\pm$ 3 km and anomalously low mantle shear velocities to depths of 45 km. *Chave* [1979] attributed the low-velocity mantle to a geochemical heterogeneity. Low mantle shear velocities imply low-density mantle, and/or more partial melting, but the distinction cannot be made with Rayleigh wave data alone [*Chave*, 1979]. However, if the low shear velocities indicate a mantle root, then our results overestimate the depth of the root, and to a lesser extent the crustal thickness. There are uncertainties in the depths determined by the seismic inversion method though that may account for these discrepancies. In addition, we do not vary the density values of the two-layer Airy model for the different plateaus, when it is likely that slightly different densities would better represent each feature and thus produce estimates of compensation depths that match the seismic determinations more closely. *Angevine and Turcotte* [1983] suggested that a model similar to that for the Agulhas Plateau may also hold for the Walvis Ridge; our results are consistent with this observation.

It has been proposed that the Crozet Plateau and south

Madagascar Ridge have a common origin at the Southwest Indian Ridge, where they were generated by excessive volcanism and subsequently split apart by seafloor spreading [*Goslin et al.*, 1981]. The Crozet Plateau is believed to be shallowly compensated [*Goslin and Patriat*, 1984], and indeed, seismic refraction locates the Moho at a depth of 17.5 km [*Goslin et al.*, 1981]. This is shallower than the 23 km Moho depth predicted by simple Airy compensation, and the 1.5 m/km geoid/topography ratio is too high. Using the two-layer Airy model, we find that crust 18.5 km thick (nearly the observed Moho depth) overlying a mantle root extending to a depth of 55 km predicts the observed geoid/topography ratio. We therefore suggest that the Crozet Plateau may be compensated by thickened crust and an anomalous low-density mantle root, similar to models for the Agulhas Plateau and Walvis Ridge. The south Madagascar Ridge, on the other hand, is deeply compensated [*Goslin et al.*, 1981], and its high geoid/topography ratio (2.3 m/km) has been attributed to recent thermal rejuvenation of the lithosphere [*Sandwell and MacKenzie*, 1989].

We investigate the north Kerguelen Plateau because, as in the features discussed above, the geoid/topography ratio is high (2.1 m/km) and the seismically determined Moho depth is shallow (14-17 km) [*Recq and Charvis*, 1986] when compared with predictions from the simple Airy model. Using the two-layer Airy model, we compute a Moho depth of 19.5 km, which is slightly deeper than observed, and a mantle root extending to a depth of 81 km. The deep mantle root may be the low-velocity (low-density) mantle anomaly beneath the Kerguelen Plateau that is indicated by deep seismic refraction and gravity data [*Recq and Charvis*, 1986]. Our results therefore agree with the findings of *Recq and Charvis* [1986] that the Kerguelen Plateau is locally compensated by a combination of crustal thickening and low-density mantle. The north Kerguelen Plateau and Broken Ridge were juxtaposed at the Southeast Indian Ridge until approximately 42 Ma, when they were rafted apart by seafloor spreading [*Mutter et al.*, 1985]. These features probably owe their origin to anomalously large basalt production at the spreading ridge [*Goslin and Patriat*, 1984]. The Broken Ridge, however, is associated with only a slightly higher geoid/topography ratio and a slightly shallower Moho depth [*Francis and Raitt*, 1967] than is predicted by simple Airy compensation.

Other oceanic plateaus have geoid/topography ratios higher than predicted by simple Airy compensation. The Caroline Seamounts, for example, have a geoid/topography ratio of 1.8 m/km. We suggest that the high ratio for this feature reflects a combination of thermal compensation in the lower lithosphere and Airy compensation of the volcanic edifices. This is consistent with the results of geochemical and age studies that indicate the seamounts were formed by passage of the lithosphere over a young hotspot or melting anomaly [*Mattey*, 1982].

The Chatham Rise and South Tasman Rise are continental plateaus that display unusually high geoid/topography ratios. *Sandwell and MacKenzie* [1989] attributed the high geoid/topography ratio of the Chatham Rise to the remnant thermal contribution of a volcanic trend that crosses the plateau [*Adams*, 1983]. The high geoid/topography ratio for the South Tasman Rise probably reflects the scatter of the data (the error is nearly 1.5 m/km). Other continental plateaus such as the Campbell and north Mascarene plateaus have geoid/topography ratios somewhat higher than that predicted by the simple Airy model for a crustal density of 2800 kg m^{-3}. Because of their continental nature, these ratios are better modeled by a simple Airy model with slightly higher density crust (~2900 kg m^{-3}). The oceanic plateaus modeled by the two-layer Airy model, however, cannot be explained by reasonable increases in crustal density.

The north Madagascar Ridge has been investigated through seismic refraction and gravity modeling [*Goslin et al.*, 1981]. Unlike the southern part, the northern portion of the ridge is in isostatic equilibrium, apparently achieved through crustal thickening. The Moho depth determined from gravity modeling matches that located by seismic refraction (25 km); however, an abnormally dense crustal root (3050 kg m^{-3}) is indicated [*Goslin et al.*, 1981]. Thus the high 1.6 m/km geoid/topography ratio of the north Madagascar Ridge probably reflects simple Airy compensation of this deep, unusually high density crustal root.

The geoid/topography ratio of the Ontong-Java Plateau lies within the group composed of thermal swells (Figure 5). *Sandwell and MacKenzie* [1989] attribute this high ratio to contamination of the compensation signal by the flexural wavelength of old lithosphere (95-110 Ma) that is bending as the plateau collides with the Solomon Islands. The Nazca Ridge exhibits a ratio even higher than predicted by the two-layer Airy model (Figure 5). We suggest that the geoid signal may likewise be contaminated, by bending of the Pacific plate as it is subducted beneath South America.

Finally, the geoid/topography ratios we obtained for the thermal swells are higher than those computed by *Sandwell and MacKenzie* [1989]. The high ratios associated with the Hawaiian and Cape Verde swells (4.6 and 4.8 m/km, respectively) more closely match those predicted by full spectral methods [*Courtney and White*, 1986; *McNutt and Shure*, 1986]. For the Hawaiian Swell, the geoid/topography ratio increased significantly from the 3.8 m/km yielded by the traditional least squares method. Significant increases from low to intermediate geoid/topography ratios are also noted for the Austral, Bermuda, Line, and Marquesas swells. These intermediate geoid/topography ratios are consistent with a combination of decaying thermal compensation in the lower lithosphere and shallow Airy compensation of the volcanic edifice.

SUMMARY

We have analyzed the relationship between geoid height and topography for 53 oceanic plateaus and swells that were previously investigated by *Sandwell and MacKenzie* [1989]. We used a nonbiased linear regression method (functional analysis) to compute the geoid/topography ratios because uncertainties are contained in both geoid height and topography data. This nonbiased linear regression method yields slopes that are systematically higher than those obtained from the traditional least squares method, where all the uncertainties are assumed to reside in the geoid height data.

We find that thermal swells are associated with intermediate to high geoid/topography ratios (~2-6 m/km) and low plateau heights (<3 km), while oceanic and continental plateaus display lower ratios (0-2 m/km) for a wide range of plateau heights (1-5.5 km). Approximately half of the oceanic and continental plateaus have low geoid/topography ratios that are in agreement with Airy crustal thickening. The remaining plateaus, however, have geoid/topography ratios that are significantly higher than predicted by the simple Airy model, and the seismically determined Moho depths beneath some of these features are too shallow for thickened crust alone. A two-layer Airy compensation model, composed of thickened crust underlain by an anomalously low density "mantle root" [*Angevine and Turcotte*, 1983], was used to explain these observations.

The Walvis Ridge and the Agulhas, Crozet, and north

Kerguelen plateaus have geoid/topography ratios and Moho depths that are consistent with the two-layer Airy compensation model. This indicates that each of these features is compensated by some combination of crustal and mantle root. The low-density mantle roots beneath these features may be regions of depleted mantle. The proximity of the Agulhas Plateau to a RRR triple junction during its early development, and the excessive volcanism at active spreading ridges that created the Crozet and north Kerguelen plateaus and the Walvis Ridge, can produce regions of enhanced depletion and hence the low-density mantle anomalies. If this explanation is correct, then the low-density mantle anomaly persists over time and remains embedded in the lithosphere beneath the oceanic feature.

Other oceanic features having geoid/topography ratios higher than predicted by Airy compensation, such as the Caroline Seamounts and south Madagascar Ridge, are explained by partial thermal compensation due to reheating of the lithosphere. The slightly higher ratios over continental plateaus, however, are better modeled by simple Airy compensation of slightly higher density crust (~2900 kg m^{-3}). The geoid/topography ratios for the thermal swells are significantly higher than those computed using traditional least squares regression.

Acknowledgments. We thank James Marsh for providing the gridded Seasat data and Richard Rapp for providing the spherical harmonic coefficients for topography. K.M.M. thanks Scripps Institution of Oceanography for the use of their facilities.

REFERENCES

Adams, C., Age of the volcanoes and granite basement of the Auckland Islands, southwest Pacific, *N. Z. J. Geol. Geophys.*, *26*, 227-237, 1983.

Angevine, C. L., and D. L. Turcotte, Correlation of geoid and depth anomalies over the Agulhas Plateau, *Tectonophysics, 100*, 43-52, 1983.

Bowin, C. O., Depth of principal mass anomalies contributing to the Earth's geoidal undulations and gravity anomalies, *Mar. Geod., 7*, 61-100, 1983.

Chave, A. D., Lithospheric structure of the Walvis Ridge from Rayleigh wave dispersion, *J. Geophys. Res., 84*, 6840-6848, 1979.

Courtney, R. C., and R. S. White, Anomalous heat flow and geoid across the Cape Verde Rise: Evidence for dynamic support from a thermal plume in the mantle, *Geophys. J. R. Astron. Soc., 87*, 815-867, 1986.

Deming, W. E., *Statistical Adjustment of Data*, 261 pp., John Wiley, New York, 1943.

Dick, H. J. B., R. L. Fisher, and W. B. Bryan, Mineralogic variability of the uppermost mantle along mid-ocean ridges, *Earth Planet. Sci. Lett., 69*, 88-106, 1984.

Francis, T. J. G., and R. W. Raitt, Seismic refraction measurements in the southern Indian Ocean, *J. Geophys. Res., 72*, 3015-3041, 1967.

Goslin, J., and P. Patriat, Absolute and relative plate motions and hypotheses on the origin of five aseismic ridges in the Indian Ocean, *Tectonophysics, 101*, 221-244, 1984.

Goslin, J., M. Recq, and R. Schlich, Structure profonde du plateau de Madagascar: Relations avec le plateau de Crozet, *Tectonophysics, 76*, 75-97, 1981.

Haxby, W. F., and D. L. Turcotte, On isostatic geoid anomalies, *J. Geophys. Res., 83*, 5473-5478, 1978.

Jones, T. A., Fitting straight lines when both variables are subject to error, I: Maximum likelihood and least squares estimations, *Math. Geol., 11*, 1-25, 1979.

Kermack, K. A., and B. S. Haldane, Organic correlation and allometry, *Biometrics, 9*, 47-58, 1950.

Mark, D. M., and M. Church, On the misuse of regression in earth science, *Math. Geol., 9*, 63-75, 1977.

Marsh, J. G., A. C. Brenner, B. D. Beckley, and T. V. Martin, Global mean sea surface based on the Seasat altimeter data, *J. Geophys. Res., 91*, 3501-3506, 1986.

Mattey, D., Minor and trace element geochemistry of volcanic rocks from Truk, Ponape, and Kusaie, eastern Caroline Islands: Evolution of a young hot spot trace across old oceanic crust, *Contrib. Mineral. Petrol., 80*, 1-13, 1982.

McNutt, M., and L. Shure, Estimating the compensation depth of the Hawaiian Swell with linear filters, *J. Geophys. Res., 91*, 13,915-13,923, 1986.

Mutter, J. C., K. A. Hegarty, S. C. Cande, and J. K. Weissel, Breakup between Australia and Antarctica: A brief review in the light of new data, *Tectonophysics, 114*, 255-279, 1985.

Ockendon, J. R., and D. L. Turcotte, On the gravitational potential and field anomalies due to thin mass layers, *Geophys. J. R. Astron. Soc., 48*, 479-492, 1977.

Oxburgh, E. R., and E. M. Parmentier, Compositional and density stratification in oceanic lithosphere - causes and consequences, *J. Geol. Soc. London, 133*, 343-355, 1977.

Recq, M., and P. Charvis, A seismic refraction survey in the Kerguelen Isles, southern Indian Ocean, *Geophys. J. R. Astron. Soc., 84*, 529-559, 1986.

Sandwell, D. T., and K. R. MacKenzie, Geoid height versus topography for oceanic plateaus and swells, *J. Geophys. Res., 94*, 7403-7418, 1989.

Tucholke, B. E., R. E. Houtz, and D. M. Barrett, Continental crust beneath the Agulhas Plateau, southwest Indian Ocean, *J. Geophys. Res., 86*, 3791-3806, 1981.

Van Wykhouse, R., SYNBAPS (Synthetic Bathymetric Profiling Systems), *Tech. Rep. TR-233*, Nav. Oceanogr. Office, Washington, DC, 1973.

York, D., Least-squares fitting of a straight line, *Can. J. Phys., 44*, 1079-1086, 1966.

K. M. Marks, National Geodetic Survey, N/CG113: GRDL, Rockville, MD 20852.

D. T. Sandwell, Scripps Institution of Oceanography, La Jolla, CA 92093.

(Received March 23, 1990;
revised December 15, 1990;
accepted January 18, 1991.)